

# Antiprotons from dark matter annihilation through light mediators and a possible excess in AMS-02 $\bar{p}/p$ data

Xian-Jun Huang, Chun-Cheng Wei, Yue-Liang Wu, Wei-Hong Zhang, and Yu-Feng Zhou  
 CAS Key Laboratory of Theoretical Physics, Institute of Theoretical Physics,  
 Chinese Academy of Sciences, ZhongGuanCun East Rd.55, Beijing, 100190, China. and  
 University of Chinese Academy of Sciences, Yuquan Rd.19A, Beijing 100049, China

We show that in the scenario where dark matter (DM) particles annihilate through light mediators, the energy spectra of the final state cosmic-ray particles depend strongly on the mediator mass. For final state antiprotons, a spectrum with relatively narrow peak occurs when the mediator mass is comparable to the  $\bar{p}p$  production threshold. Of interest, the latest AMS-02 data on the  $\bar{p}/p$  flux ratio hint at a bump-like excess over the expected background in the energy range  $\sim 100 - 450$  GeV. We show that such a light mediator scenario is favoured by the latest AMS-02 data over the scenarios of DM direct annihilation into the standard model particles and that of antiprotons produced from inside supernova remnants (SNRs), and is consistent with the upper limits derived from the Fermi-LAT data on the gamma rays towards the dwarf spheroidal galaxies. The  $\bar{p}/p$  flux ratio with energy above 450 GeV is predicted to fall with energy quickly, which can be easily distinguished from the other two scenarios as they predict the ratio to be flattening or rising up to multi-TeV region.

*Introduction.* Cosmic-ray (CR) antiparticles such as positrons and antiprotons are relatively rare and sensitive to exotic contributions. In recent years, an excess over the expected background in CR positrons has been observed [1]. The spectral feature of the excess plays an important role in identifying its origin such as nearby astrophysical sources or dark matter (DM) interactions. Recently, the AMS-02 collaboration published the measurement on the antiproton to proton ( $\bar{p}/p$ ) flux ratio up to kinetic energy 450 GeV, based on four years of data taking [2], confirming the first preliminary result presented in the year 2015 [3]. Although the measured kinetic energy spectrum of  $\bar{p}/p$  ratio is in overall agreement with the secondary production especially below  $\sim 100$  GeV [4, 5], at higher energies, there is a trend of flattening and smooth rise in the range  $\sim 100 - 260$  GeV, followed by a drop by  $\sim 30\%$  in the range  $\sim 260 - 450$  GeV. Such a hint of a bump-like excess has already been observed in the preliminary AMS-02 result [3], and is strengthened in the latest data with higher statistics.

This intriguing possibility of an excess with a distinctive spectral feature in  $\bar{p}/p$  flux ratio, if confirmed, may shed light on the nature of its origin: i) The pulsar wind nebulae are unlikely to produce energetic antiprotons. ii) In the leading astrophysical explanation, extra antiprotons can be produced from collisions of primary CRs with the gas inside supernova remnants (SNRs), the resulting energy spectrum, however, features a continued flattening or weak rise at least up to 1 TeV for a typical cut-off energy  $\mathcal{E}_{\max} \sim \mathcal{O}(10)$  TeV [6, 7]. iii) The spectrum of antiprotons produced from halo DM annihilation directly into standard model (SM) final states in general features a very broad bump due to the long chain of cascade showers and hadronization of the final state partons. Since there is little room left for extra contributions below  $\sim 100$  GeV, the DM particle mass  $m_\chi$  is pushed to be very high ( $m_\chi \gtrsim 2$  TeV) [4, 5, 8, 9]. Consequently, only

the spectral tail of DM produced antiprotons can extend to the energy range accessible to the current AMS-02 experiment ( $E \lesssim 450$  GeV), thus again a flattening or weak rise of  $\bar{p}/p$  ratio is expected in this region.

In this letter, we show that in a class of scenarios where DM particles annihilate through light color-singlet mediators, the energy spectrum of final state particle can be a narrow bump with reduced multiplicity. For antiprotons, a narrow peak occurs when the mediator mass is comparable to the  $\bar{p}p$  production threshold  $2m_p$ . We show that such a light mediator scenario is favoured by the latest AMS-02 data over the scenario of DM direct annihilation and that of antiprotons produced from inside of SNRs, and is also consistent with the known constraints such as the gamma-ray limits from the dwarf spheroidal galaxies (dSphs). The  $\bar{p}/p$  ratio in the high energy range is predicted to fall with energy quickly, which makes it highly distinguishable from the other two scenarios.

*Effects of mediators.* The annihilation of DM particles provides an extra primary source of CR particles. The corresponding primary source term for a final state particle  $f$  takes the form

$$q(\mathbf{r}, E) = \frac{\rho(\mathbf{r})^2}{2m_\chi^2} \langle \sigma v \rangle \frac{dN}{dE}, \quad (1)$$

where  $\langle \sigma v \rangle$  is the velocity-averaged DM annihilation cross section multiplied by DM relative velocity,  $\rho(\mathbf{r})$  is the DM energy density distribution function,  $dN/dE$  is the spectrum of kinetic energy  $E$  which is related to the total energy  $\mathcal{E}$  as  $E = \mathcal{E} - m_f$  with  $m_f$  the mass of the final state particle  $f$ .

In many well-motivated DM models, the DM particles do not couple to the SM particles directly, but through some light color-singlet mediator particles, which has rich phenomenological consequences in DM annihilation [10–12], self-scatterings [13–15] and solar capture [16, 17], and direct detections [18, 19]. In this scenario, for the same

DM mass, the resulting energy spectrum of final state particle from DM annihilation can be significantly different from the case without a mediator. Let us consider DM annihilating first into two mediators  $\bar{\chi}\chi \rightarrow 2\varphi$  and followed by the decay  $\varphi \rightarrow f + X$ , where  $X$  stands for any other final states. The spectrum  $dN(x)/dx$  of the scaled total energy  $x = \mathcal{E}/m_\chi$  in the DM center-of-mass frame is related to that in the mediator rest-frame  $dN(x')/dx'$  (with  $x' = 2\mathcal{E}'/m_\varphi$ ) by a Lorentz boost

$$\frac{dN(x)}{dx} = 2 \int_{a(x)}^{b(x)} dx' \frac{1}{\sqrt{1-\varepsilon_1^2} \sqrt{x'^2 - \varepsilon_0^2}} \frac{dN(x')}{dx'}, \quad (2)$$

where the two parameters  $\varepsilon_1 = m_\varphi/m_\chi$  and  $\varepsilon_0 = 2m_f/m_\varphi$  characterize the mass hierarchies in the two-step cascade process. The lower and upper limits of the integration are  $a(x) = x_-$  and  $b(x) = \min\{1, x_+\}$  with  $x_\pm = 2(x \pm \sqrt{(1-\varepsilon_1^2)(x^2 - \varepsilon_1^2\varepsilon_0^2/4)})/\varepsilon_1^2$ . In the large hierarchy limit  $\varepsilon_0 \ll 1$ , Eq. (2) reproduces the known result in Refs. [20, 21].

In general, Lorentz boosts at random directions tend to broaden the energy spectrum. However, the effect of broadening is suppressed if the velocity of  $f$  in the mediator rest-frame is small. In the simplest case where  $f$  is mono-energetic with energy  $\mathcal{E}'$ , i.e.  $dN/\mathcal{E}' \propto \delta(\mathcal{E}' - \mathcal{E}')$  in the mediator rest-frame, the spectrum boosted to the DM center-of-mass frame is a box-shaped spectrum with a center energy  $\bar{\mathcal{E}}$  and width  $\Delta\mathcal{E}$

$$\bar{\mathcal{E}} = \gamma_B \mathcal{E}', \quad \Delta\mathcal{E}/\bar{\mathcal{E}} = 2\beta_B \beta', \quad (3)$$

where  $\gamma_B = 1/\varepsilon_1$  is the Lorentz boost factor,  $\beta_B = (1-\varepsilon_1^2)^{1/2}$  is the boost velocity, and  $\beta' = (1-m_f^2/\mathcal{E}'^2)^{1/2}$  is the velocity of  $f$  in the mediator rest-frame. For the decay of mediator into light quarks  $\varphi \rightarrow \bar{q}q \rightarrow \bar{p} + X$  ( $q = u, d$ ), the velocity of antiproton has an upper limit  $\beta' \leq (1-\varepsilon_0^2)^{1/2}$  as  $X$  at least contains a proton. Thus when  $\varepsilon_0 \approx \mathcal{O}(1)$ , namely,  $m_\varphi$  is comparable to the  $\bar{p}p$  production threshold  $2m_p$ , the value of  $\beta'$  has to be small and the spectrum is a narrow box in the DM halo rest-frame. On the other hand, the total energy has a lower limit  $\mathcal{E}' \geq m_p$ , the value of  $\bar{\mathcal{E}}$  can be very large for a large Lorentz boost factor  $\gamma_B \gg 1$ . Thus after the boost, the energy spectrum is a narrow box at high energy. Since the antiproton energy spectrum from the decay  $\varphi \rightarrow \bar{q}q \rightarrow \bar{p} + X$  is low-energy dominated, the Lorentz boost will push the antiprotons into high energy region without significantly broadening the spectrum. On the contrary, the antiproton spectrum from DM direct annihilation  $\chi\chi \rightarrow \bar{q}q$  is very broad for the same DM mass, due to the larger center-of-mass energy of the  $\bar{q}q$  system and thus the longer chain of cascade parton showers and hadronization. Furthermore, in the light mediator scenario, the multiplicities of the final state particles are suppressed by the smallness of the mediator mass and can be much lower than that in the case without mediators. For the hadronic decay  $\varphi \rightarrow \bar{q}q$ , the energy

spectrum  $dN/dx'$  of antiprotons is simulated using the Monte Carlo event generator Pythia 8.2 [22]. The  $\bar{p}$  multiplicity is found to be  $N_p = 0.35, 1.2, 1.6$  and  $3.0$  for the center-of-mass energy  $\mathcal{E}_{\text{CM}} = 10, 50, 100$  and  $500$  GeV, respectively. Thus for the same DM mass, the DM annihilation through light mediators will generate less antiprotons due to lower center-of-mass energy.

In Fig. 1, we show the spectra of antiproton kinetic energy and photon energy from the annihilation  $\chi\chi \rightarrow 2\varphi \rightarrow 2(\bar{q}q)$  of a 500 GeV DM particle with three different mediator masses,  $m_\varphi = 5, 10$  and  $50$  GeV, respectively. For a comparison, the spectrum for DM direct annihilation  $\chi\chi \rightarrow \bar{q}q$  for the same DM mass is also shown. For a very light mediator  $m_\varphi = 5$  GeV, the antiproton spectrum appears to be a narrow bump. As the mediator mass increases, the spectrum becomes broader. For  $m_\varphi = 50$  GeV, the spectrum looks similar to that from DM direct annihilation, but with lower multiplicity. Similar observations hold for the photon energy spectrum. The figure illustrates that the energy spectra of antiprotons and photons from DM annihilation can be highly model dependent, which will drastically change the interpretations of the experimental data. While the predictions from Pythia for low energy hadronic processes have not been fully validated [23], the presence of the narrow-bump spectrum is a generic kinematical effect, and is insensitive to the details of hadronization model.

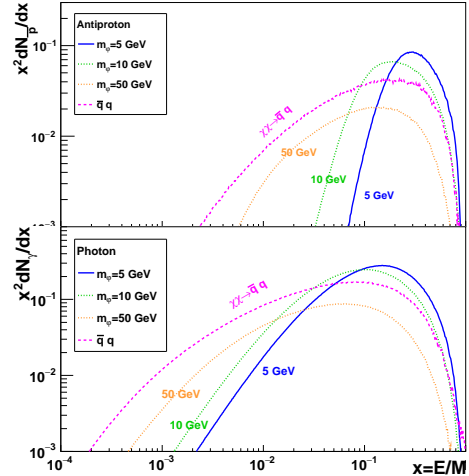


FIG. 1: Upper panel) scaled energy spectra  $x^2 dN/dx$  of antiprotons per DM annihilation from the annihilation  $\chi\chi \rightarrow 2\varphi \rightarrow 2\bar{q}q$ , ( $q = u, d$ ) with mediator masses  $m_\varphi = 5, 10$  and  $50$  GeV, respectively. The DM particle mass is fixed at  $m_\chi = 500$  GeV. The spectrum of DM direct annihilation  $\chi\chi \rightarrow \bar{q}q$  with the same DM mass is also shown. Lower panel) the same as the upper panel, but for photons.

*SNR contributions.* It has been suggested that extra secondary antiprotons can be generated from the collisions of primary CRs onto the gas inside the SNRs, and

accelerated by the shock wave in the same way as that of the primary CRs [6, 24–26]. This mechanism does not require new class of sources and predicts strong correlations between the spectra of secondary species such as positrons, antiprotons and heavy nuclei. We consider the setup in the rest-frame of the shock front (at  $x = 0$ ) where  $u_1(u_2)$  and  $n_1(n_2)$  are the upstream (downstream) plasma speed and density respectively. The compression factor  $r = u_1/u_2 = n_2/n_1$  determines the power law index  $\gamma = 3r/(r-1)$  of the primary proton spectrum. Since the secondary antiprotons are produced inside SNRs and propagate in the same ways as primary protons, which largely cancels the effect of propagation. The  $\bar{p}/p$  flux ratio from solving the transportation equation for  $\bar{p}$  inside SNRs is given by [6]

$$\left(\frac{\Phi_{\bar{p}}}{\Phi_p}\right)_{\text{SNR}} \sim 2n_1c \left[ \gamma \left( \frac{1}{\xi} + r^2 \right) \int_{m_p}^{\mathcal{E}} d\omega \omega^{\gamma-3} \frac{D_1(\omega)}{u_1^2} I(\omega) + \frac{\tau_{\text{SNR}} r}{2\mathcal{E}^{2-\gamma}} I(\mathcal{E}) \right], \quad (4)$$

where the first (second) term in the square brackets corresponds to the generation of  $\bar{p}$  with (without) acceleration. The source function  $I$  is defined as  $I(\omega) = \int_{\omega}^{\mathcal{E}_{\text{max}}} d\varepsilon \varepsilon^{2-\gamma} \sigma(\varepsilon, \omega)$ , where  $\sigma(\varepsilon, \omega)$  is the  $\bar{p}$  production cross section for the process  $p(\varepsilon) + \text{H} \rightarrow \bar{p}(\omega) + X$ , which is taken from [27]. The parameter  $\xi$  is the fraction of proton energy carried away by a secondary antiproton, and  $\tau_{\text{SNR}}$  is the typical SNR age. The diffusion coefficient upstream is  $D_1(\mathcal{E}) \simeq 3.3 \times 10^{22} \mathcal{F}^{-1} (\mathcal{E}/\text{GeV}) (B/\mu\text{G})^{-1} \text{cm}^2 \text{s}^{-1}$ . In the numerical calculation, we fix the parameters as  $u_1 = 0.5 \times 10^8 \text{ cm} \cdot \text{s}^{-1}$ ,  $n_1 = 2 \text{ cm}^{-3}$ ,  $r = 3.8$ ,  $\xi = 0.17$ , and  $\tau_{\text{SNR}} = 2 \times 10^4 \text{ yr}$ . For the parameters in the diffusion coefficients, we fix them as  $\mathcal{F} = 1/20$  and  $B = 1 \mu\text{G}$ . Note that the normalization of the  $\bar{p}/p$  ratio is proportional to the combination  $N_{\text{SNR}} = n_1 u_1^{-2} B_{\mu\text{G}}^{-1} \mathcal{F}^{-1}$ . There are some uncertainties in the cut-off energy  $\mathcal{E}_{\text{max}}$  which depends on the typical SNR age, but the typical value is  $\mathcal{E}_{\text{max}} \approx \mathcal{O}(10 - 100) \text{ TeV}$  [6, 7]. From Eq. (4), one can see that the  $\bar{p}/p$  flux ratio increases monotonously with increasing energy  $E$  and saturates when  $\mathcal{E} \approx \mathcal{E}_{\text{max}}$ . Thus the generic prediction of the model is a flattening and eventually a rise of the  $\bar{p}/p$  ratio in the 100 GeV – multi-TeV region.

*Fit to AMS data.* We compare the above-mentioned three scenarios of antiproton production: A) DM annihilation into quarks through light mediators, B) DM direct annihilation into quarks, and C) antiprotons produced from the inside of SNRs through fitting to the high energy AMS-02 antiproton data and examine whether they are favoured and can be distinguished by the current and future experiments. The propagation of the CR antiprotons is calculated using GALPROP v54 [28]. We consider three representative propagation models selected from a global Bayesian analysis to the AMS-02 proton and B/C data using the GALPROP code [29]. They are selected

to represent the typically minimal (MIN), median (MED) and maximal (MAX) antiproton fluxes at 95% C.L.. Note that these propagation models are different from and complementary to that given in Ref. [30] which are based on semi-analytical solutions with simplified assumptions. The Einasto DM profile is adopted as a benchmark profile with a local DM density of  $\rho_0 = 0.43 \text{ GeV cm}^{-3}$ . The effect of solar modulation is taken into account using the force-field approximation [31]. We use charge asymmetric Fisk potentials  $\phi_p = 550 \text{ MV}$  and  $\phi_{\bar{p}}/\phi_p = 0.2$  which leads to a good agreement with the low-energy antiproton data [32].

We determine the model parameters through fitting to the AMS-02 data. Since we are only interested in the high energy part of the  $\bar{p}/p$  spectrum, only the  $\bar{p}/p$  data with  $E \geq 20 \text{ GeV}$  (in total 26 data points) are included, which also largely avoids the uncertainties in modelling the solar modulation. Discussions on a possible  $\bar{p}$  excess at low energies can be found in Refs. [5, 32, 33]. The significance of an excess over the background is estimated using a test statistics  $\text{TS} = -2 \ln(\mathcal{L}_{\text{bg}}/\mathcal{L}_{\text{bg+src}})$ , where  $\mathcal{L}_{\text{bg}}$  and  $\mathcal{L}_{\text{bg+src}}$  are the likelihood functions for the scenarios of background-only and background plus extra sources, respectively. In all the fits, the normalization of the secondary background is allowed to float freely, i.e.  $\Phi_{\bar{p},bg} \rightarrow \kappa \Phi_{\bar{p},bg}$  with the normalization constant  $\kappa$  determined solely by data.

The fit to the data in the background-only scenario in the MED propagation model results in  $\chi^2 = 22.8$  for 25 degrees-of-freedom(d.o.f.), suggesting a good agreement with the data. The best-fit background of  $\bar{p}/p$  ratio is shown in Fig. 2. Despite the over agreement, a hint of systematic deviation at energies above  $\sim 100 \text{ GeV}$  can be seen clearly. The best-fit backgrounds in the MIN and MAX models are found to be very close to that in the MED model.

In the scenario A, i.e.,  $\chi\chi \rightarrow 2\varphi \rightarrow 2\bar{q}q$ , we first consider the case of a 5 GeV mediator. The best-fit parameters,  $\chi^2$  and TS values are summarized in Tab. I. In the three propagation models, the favoured DM masses are in the range 600 GeV – 1 TeV. In the MED model, the best-fit cross section is compatible with the typical thermal cross section. From the MIN to the MAX model, the variation of the best-fit cross section is within an order of magnitude, which represents the typical uncertainties due to propagation models. Since the measured  $\bar{p}/p$  is very small and of  $\mathcal{O}(10^{-4})$ , it is a good approximation that the background and the new source contributions can be summed together in  $\bar{p}/p$  flux ratio, i.e.,  $\Phi_{\bar{p}}/\Phi_p \approx (\Phi_{\bar{p},bg}/\Phi_p) + (\Phi_{\bar{p},src}/\Phi_p)$ . In Fig. 2, the best-fit  $\bar{p}/p$  flux ratios together with the background in the MED model are shown. It can be seen that the structure in the AMS-02 data at  $\sim 300 \text{ GeV}$  can be reproduced for  $m_\varphi = 5 \text{ GeV}$ . For heavier mediators, we find  $m_\chi = 1.49(2.74) \text{ TeV}$ ,  $\langle\sigma v\rangle = 9.4(23.2) \times 10^{-26} \text{ cm}^3 \text{s}^{-1}$  and  $\chi^2 = 14.3(14.9)$  for  $m_\varphi = 10(20) \text{ GeV}$ , and the

peaks of the best-fit spectra move to higher energies, which worsens the agreement with the data, and results in larger  $\chi^2$  values, as can be seen from Fig. 2.

	Model	$m_\chi$ [GeV]	$\langle\sigma v\rangle(\eta)$	$\kappa$	$\chi^2$	TS
A	MIN	$765^{+167}_{-153}$	$18.6^{+10.7}_{-8.0}$	$1.12\pm 0.01$	12.5	11.6
	MED	$808^{+184}_{-165}$	$5.18^{+3.04}_{-2.37}$	$1.13\pm 0.01$	13.8	9.0
	MAX	$826^{+185}_{-168}$	$2.29^{+1.31}_{-1.06}$	$1.13\pm 0.01$	15.5	8.5
B	MIN	20000	$1200\pm 410$	$1.12\pm 0.01$	15.5	8.6
	MED	20000	$291\pm 123$	$1.13\pm 0.01$	17.2	5.6
	MAX	20000	$117\pm 54$	$1.12\pm 0.01$	19.3	4.7
C	MIN	—	$(0.262\pm 0.103)$	$1.08\pm 0.02$	17.6	6.5
	MED	—	$(0.195\pm 0.104)$	$1.10\pm 0.02$	19.2	3.5
	MAX	—	$(0.172^{+0.104}_{-0.105})$	$1.10\pm 0.02$	21.4	2.7

TAB. I: Fit results for the three scenarios: scenario A with  $m_\varphi = 5.0$  GeV, scenario B with  $m_\chi = 20$  TeV, and scenario C with  $\mathcal{E}_{\max} = 10$  TeV, in the MIN, MED and MAX propagation models. The cross section is in units of  $10^{-26}\text{cm}^3\text{s}^{-1}$ . The numbers in the parentheses in the scenario C stand for the values of the factor  $\eta$ .

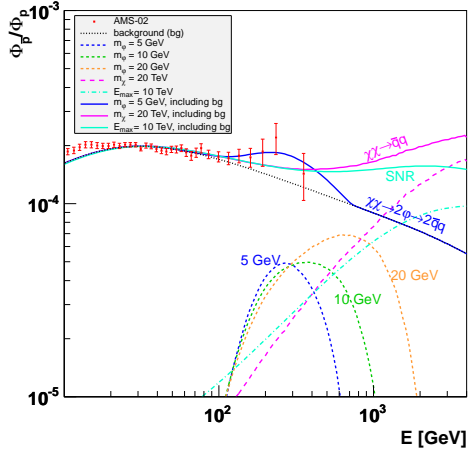


FIG. 2: Best-fit  $\bar{p}/p$  flux ratios from the three scenarios: scenario A with mediator mass  $m_\varphi = 5, 10$  and  $20$  GeV, respectively, scenario B with  $m_\chi = 20$  TeV, and scenario C with  $\mathcal{E}_{\max} = 10$  TeV. The sum with the background in each scenario (for  $m_\varphi = 5$  GeV in scenario A) is also shown, together with the AMS-02 data [2].

In the scenario B, i.e.,  $\chi\chi \rightarrow \bar{q}q$ , we find that the current data impose a lower limit of  $m_\chi \gtrsim 2$  TeV, confirming the previous analysis based on the preliminary data [5]. Introducing a heavier DM mass always improves the agreement with the data. However, after  $m_\chi \gtrsim 10$  TeV, the value of  $\chi^2$  gradually ceases to decrease and approaches a constant. The reason is that for very heavy DM particles, only the low-energy tail of the DM generated antiproton spectrum can extend to the region accessible to the current AMS-02 experiment

( $E \leq 450$  GeV). In this region, the increase of the DM mass leads to lower  $\bar{p}$  flux which can be compensated by the increase of the annihilation cross section. In Tab. I, the fit results for fixed  $m_\chi = 20$  TeV are shown. The corresponding best-fit  $\bar{p}/p$  ratio is shown in Fig. 2.

For the scenario C, we use the expression of Eq. (4) plus a background contribution. Besides the normalization factor  $\kappa$  of the background, the normalization of SNR contribution is also allowed to vary freely by introducing a factor  $\eta$ , i.e.,  $N_{\text{SNR}} \rightarrow \eta N_{\text{SNR}}$ . The spectral shape of the SNR antiprotons is characterized by the maximal energy  $\mathcal{E}_{\max}$ . Similar to the case of the DM direct annihilation, we find that a SNR contribution with sufficiently large  $\mathcal{E}_{\max} \sim \mathcal{O}(10)$  TeV can improve the agreement with the data, and the improvement gradually saturates when  $\mathcal{E}_{\max} \gtrsim 10$  TeV, which is due to a similar degeneracy between  $\mathcal{E}_{\max}$  and the normalization factor  $\eta$ . We thus fix the cut-off  $\mathcal{E}_{\max}$  to be 10 TeV. The predicted spectrum of  $\bar{p}/p$  ratio in the multi-TeV region is again a flattening and weak rise until the maximum energy  $\mathcal{E}_{\max}$  is reached.

The TS values of the three scenarios in the three propagation models are listed in Tab. I. It is clear that the scenario A has the highest significance in all the propagation models. In this scenario, as can be seen from Fig. 2, above 450 GeV, the  $\bar{p}/p$  ratio is expected to fall with energy, while in the other two scenarios, the spectra will continue to rise to higher energies. Thus this scenario can be distinguished easily from the other two by the future data.

*Constraints.* The most stringent and robust constraints so far on the DM annihilation cross sections arise from the observation of  $\gamma$ -rays towards dSphs by the Fermi-LAT collaboration [34]. Due to the significant difference in the spectra shape, the reported Fermi-LAT limits do not apply to the case where DM annihilates through mediators. We derive the upper limits directly from the likelihood profile per energy bin of gamma-rays provided by the Fermi-LAT collaboration for a selection of 15 dSphs with high-confidence J-factors and backgrounds [35]. As a cross check, in Fig. 3 we show the derived upper limits for the DM direct annihilation  $\chi\chi \rightarrow \bar{q}q$  which well reproduces result of Fermi-LAT [34]. The limits for the case with  $m_\varphi = 5, 10$  and  $20$  GeV are shown in Fig. 3, together with the regions allowed by the AMS-02 data. The favoured regions are all consistent with the current limits. The derived upper limits turn out to be dependent on the mediator mass at high DM mass region. Compared with the direct DM annihilation, we find that at high energies around 10 TeV, the derived upper limit is weaker by a factor of five. This is due to the fact that for a multi-TeV DM particle, the relatively narrow  $\gamma$ -ray spectrum shown in Fig. 1 has smaller fraction of photons entering into the low energy region accessible to Fermi-LAT experiment, which results in less stringent constraints.

In the scenario of DM annihilation into light quarks



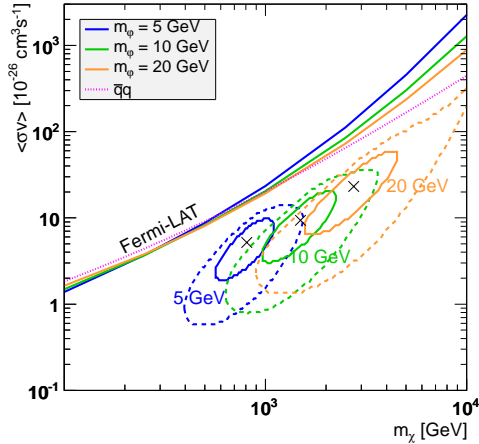


FIG. 3: Contours of favoured regions by the AMS-02 data at 68% (solid) and 95% (dashed) C.L.s. in  $(m_\chi, \langle\sigma v\rangle)$  plane in the scenario A with  $m_\phi = 5, 10$  and  $20$  GeV, respectively. The crosses indicate the best-fit values. The 95% C.L. upper limits derived from the Fermi-LAT data on the dSphs are shown as the solid curves. The derived limits for the scenario B are also shown.

through mediators, we find that the predicted positron fraction is at most  $4 \times 10^{-4}$  for  $m_\phi = 5$  GeV, which is far below the expected background  $\sim \mathcal{O}(10^{-2})$  [29, 36]. Thus the constraints from the positron fraction is rather weak. The current LHC search for mono-X plus missing energy can only impose constraints on the mediator mass in the case of  $m_\phi > 2m_\chi$  [37], which makes it less relevant to the case of DM annihilation with light mediators.

*Acknowledgements.* YLW is grateful to S. Ting for warm hospitality and discussions during his visit to the AMS-02 collaboration at CERN. This work is supported by the NSFC under Grants No. 11335012 and No. 11475237.

[1] O. Adriani *et al.*, *Astropart. Phys.* **34**, 1 (2010); M. Ackermann *et al.* [Fermi-LAT Collaboration], *Phys. Rev. Lett.* **108**, 011103 (2012); L. Accardo *et al.* [AMS Collaboration], *Phys. Rev. Lett.* **113**, 121101 (2014).  
[2] M. Aguilar *et al.* (AMS), *Phys. Rev. Lett.* **117**, 091103 (2016).  
[3] S. Ting, talk at *AMS-02 days at CERN*, April 15-17, CERN, Geneva.  
[4] G. Giesen, M. Boudaud, Y. Gnolini, V. Poulin, M. Cirelli, P. Salati, and P. D. Serpico, *JCAP* **1509**, 023 (2015), 1504.04276.  
[5] H.-B. Jin, Y.-L. Wu, and Y.-F. Zhou, *Phys. Rev.* **D92**, 055027 (2015), 1504.04604.  
[6] P. Blasi and P. D. Serpico, *Phys. Rev. Lett.* **103**, 081103 (2009), 0904.0871.  
[7] P. Mertsch and S. Sarkar, *Phys. Rev.* **D90**, 061301 (2014), 1402.0855.

[8] S.-J. Lin, X.-J. Bi, P.-F. Yin, and Z.-H. Yu (2015), 1504.07230.  
[9] M. Ibe, S. Matsumoto, S. Shirai, and T. T. Yanagida, *Phys. Rev.* **D91**, 111701 (2015), 1504.05554.  
[10] J. Hisano, S. Matsumoto and M. M. Nojiri, *Phys. Rev. Lett.* **92**, 031303 (2004); N. Arkani-Hamed, D. P. Finkbeiner, T. R. Slatyer and N. Weiner, *Phys. Rev. D* **79**, 015014 (2009); J. L. Feng, M. Kaplinghat and H. B. Yu, *Phys. Rev. Lett.* **104**, 151301 (2010);  
[11] Z.-P. Liu, Y.-L. Wu, and Y.-F. Zhou, *Phys. Rev.* **D88**, 096008 (2013), 1305.5438.  
[12] J. Chen and Y.-F. Zhou, *JCAP* **1304**, 017 (2013), 1301.5778.  
[13] A. Loeb and N. Weiner, *Phys. Rev. Lett.* **106**, 171302 (2011), 1011.6374.  
[14] S. Tulin, H.-B. Yu, and K. M. Zurek, *Phys. Rev. Lett.* **110**, 111301 (2013), 1210.0900.  
[15] M. Kaplinghat, T. Linden, and H.-B. Yu, *Phys. Rev. Lett.* **114**, 211303 (2015), 1501.03507.  
[16] J. Chen, Z.-L. Liang, Y.-L. Wu, and Y.-F. Zhou, *JCAP* **1512**, 021 (2015), 1505.04031.  
[17] Z.-L. Liang, Y.-L. Wu, Z.-Q. Yang, and Y.-F. Zhou, *JCAP* **1609**, 018 (2016), 1606.02157.  
[18] T. Li, S. Miao, and Y.-F. Zhou, *JCAP* **1503**, 032 (2015), 1412.6220.  
[19] E. Del Nobile, M. Kaplinghat, and H.-B. Yu, *JCAP* **1510**, 055 (2015), 1507.04007.  
[20] J. Mardon, Y. Nomura, D. Stolarski, and J. Thaler, *JCAP* **0905**, 016 (2009), 0901.2926.  
[21] G. Elor, N. L. Rodd, and T. R. Slatyer, *Phys. Rev.* **D91**, 103531 (2015), 1503.01773.  
[22] T. Sjostrand, S. Mrenna, and P. Z. Skands, *Comput. Phys. Commun.* **178**, 852 (2008), 0710.3820.  
[23] D. Muller, [BaBar Collaboration], arXiv:1310.0520 [hep-ex].  
[24] P. Mertsch and S. Sarkar, *Phys. Rev. Lett.* **103**, 081104 (2009), 0905.3152.  
[25] E. G. Berezhko and L. T. Ksenofontov, *Astrophys. J.* **791**, L22 (2014), 1405.5281.  
[26] M. Kachelrie, A. Neronov, and D. V. Semikoz, *Phys. Rev. Lett.* **115**, 181103 (2015), 1504.06472.  
[27] L. C. Tan and L. K. Ng, *Phys. Rev.* **D26**, 1179 (1982).  
[28] A. W. Strong and I. V. Moskalenko, *Astrophys. J.* **509**, 212 (1998), astro-ph/9807150.  
[29] H.-B. Jin, Y.-L. Wu, and Y.-F. Zhou, *JCAP* **1509**, 049 (2015), 1410.0171.  
[30] F. Donato, N. Fornengo, D. Maurin, and P. Salati, *Phys. Rev.* **D69**, 063501 (2004), astro-ph/0306207.  
[31] L. J. Gleeson and W. I. Axford, *Astrophys. J.* **154**, 1011 (1968).  
[32] D. Hooper, T. Linden, and P. Mertsch, *JCAP* **1503**, 021 (2015), 1410.1527.  
[33] M.-Y. Cui, Q. Yuan, Y.-L. S. Tsai, and Y.-Z. Fan (2016), 1610.03840.  
[34] M. Ackermann *et al.* (Fermi-LAT), *Phys. Rev. Lett.* **115**, 231301 (2015), 1503.02641.  
[35] L. M. Carpenter, R. Colburn, J. Goodman, and T. Linden, *Phys. Rev.* **D94**, 055027 (2016), 1606.04138.  
[36] H.-B. Jin, Y.-L. Wu, and Y.-F. Zhou, *JCAP* **1311**, 026 (2013), 1304.1997.  
[37] M. Aaboud *et al.* [ATLAS Collaboration], *Phys. Rev. D* **94**, no. 3, 032005 (2016); CMS-PAS-EXO-16-037.